Density Functional Theory Study of Selenium-Substituted Low-Bandgap Donor-Acceptor-Donor Polymer

Habib Ullah[*,†], *Salma Bibi*[‡], *Asif A. Tahir*[*,†], *and Tapas K. Mallick*[†]

[†]Environment and Sustainability Institute (ESI), University of Exeter, Penryn Campus, Penryn, Cornwall TR10 9FE, UK

[‡]National Centre of Excellence in Physical Chemistry, University of Peshawar, 25120 Peshawar, Pakistan

Corresponding Authors:

habib_chemist@yahoo.com; hu203@exeter.ac.uk (H. Ullah)

A.Tahir@exeter.ac.uk (A.A. Tahir)

Abstract

Theoretical study of an optically transparent, near-infrared-absorbing low energy gap conjugated polymer, donor−acceptor−donor (**D-A-D**); 2,1,3-benzosele-nadiazole (**A**) as acceptor and 3,4-ethylenedioxyselenophene (**D**) as donor fragments, with promising attributes for photovoltaic application is reported herein. The **D** and **A** moiety on the polymeric backbone have been found to be responsible for tuning the band gap, optical gap, open circuit (Voc) and short-circuit current density (Jsc) in the polymers solar cells (PSC). **D-A-D** has a key role in charge separation and molecular architecture which ultimately influences the charge transport. Reduction in the band gap, high charge transformation, and enhanced visible light absorption in the **D-A-D** system is because of strong overlapping of molecular orbitals of **D** and **A**. The polaron and bi-polaron effects are also investigated which has a direct relation with visible light photocurrent generation. In addition, the enhanced planarity and weak steric hindrance between adjacent units of **D-A-D**, resulted in red-shifting of its onset of absorption. The simulated band gap of the **D-A-D** has excellent correlation with experimentally reported values for closely related systems, which validates the level of theory used. Finally, PSC properties of the designed **D-A-D** was modeled in the bulk heterojunction solar cell, which gives theoretical Voc of about 1.02 eV.

1. INTRODUCTION

Solar energy harvesting is one the challenging tasks to current renewable energy scientists. Researchers are struggling for designing a cheap, liable, elastic, and environmental friendly optoelectronic devices with high efficiency.[1-4] Silicon-based materials are ideal in the current solar cells technology but having a high cost, high operation temperature; limits its portability and versatility.[5] A step toward the development of low-cost, environmentally friendly, easily synthesizable, flexible and efficient material for solar cells lead scientists to the use of conjugated organic polymers (COPs).[4,6] COPs are emerging as promising materials due to their stability, low-cost processing and ability to form tunable and robust structures. Four prominent generations of COPs are being explored by scientists, which has application in the field of solar to power energy conversion.[7-11]

COPs have tunable band gap where one can precisely tune the desired band gap, HOMO, and LUMO energy levels during the synthesis, which directly affect the open circuit voltage (V_{oc}), charge transport (η_{cT}) and short-circuit current density (J_{sc}) in the polymer solar cell (PSC).[4] Generally, polymer with a band gap of more than 4 eV is considered to be insulator while the underneath represents semiconducting nature.[12] Since the discovery of the conducting nature of polyacetylene (PA), researchers are working to minimize this band gap.[13] Many efforts are reported in this regards which are either, co-polymerization, composites, nanoparticles, and donor-acceptor co-polymerization.[14]

The major issues with PSCs are their low efficiency in the photovoltaic devices which links to the incident photon to electron conversion. To date, the power conversion efficiency (PCE) of PSC has been enhanced up to 13.2%,[15,16] means still large efforts are being required of making it acceptable all over the world. As explained elsewhere,[4] the conduction mechanism of the PSC is also different from that of inorganic semiconductors. Other problem associated with the

PSC is large exciton binding energy which requires the high energy of dissociation into electron and hole and thus results in less efficiency of the organic based PSC.[17] Finally, COPs used in the PSC should have the ability to absorb the visible part of the solar spectrum (narrow band gap) and a well below HOMO energy level compared to the LUMO of Phenyl-C_{61}-butyric acid methyl ester (PCBM), used in the bulk heterojunction.

COPs monomers such as *3,4*-ethylenedioxythiophene (EDOT) and *3,4*-ethylenedioxyselenophene (EDOS) are working as a donor while *2,1,3*-bezothiadizole (BOD) and *2,1,3*-benzoselenadiazole (BSD) moieties act as an acceptor in the donor-acceptor combination (Scheme S1). Synthetic mechanism and electropolymerization of EDOS into poly *3,4*-ethylenedioxyselenophene (PEDOS) are given in Fig S1 and S2, respectively while that of poly *3,4*-ethylenedioxythiophene (PEDOT), poly *2,1,3*-benzoselenadiazole (PBSD), and poly *2,1,3*-bezothiadizole (PBOD) can be found elsewhere.[18]

To overcome the challenges of PSC, a donor-acceptor approach has been using to efficiently tune the HOMO-LUMO levels and optical band gap.[19-23] As we know, the processes are not so simple, requires a lot of efforts to get insight into the underlying phenomenon.[17] The combination of the donor (electron donating species) and acceptor moieties (electron withdrawing) in a copolymer can tune the optical gap and efficiently harness the solar energy influx which is consequently responsible for the increase of *Jsc*. This would not simply solve our problem but band gap engineering of a polymer can lead to increase the *Voc*, followed by efficient exciton dissociation in the PSC.[24]

The purpose of this work is to design and suggest such a polymer that can be used in the bulk heterojunction (organic solar cell), having enhanced *Voc*, *Jsc*, and fill factor (FF).[25] In this work, we used different conjugated organic monomer having donors and acceptors nature which can give rise to a low band gap polymer with desired bandwidth positions. More

4

interestingly, these exciting materials are rarely investigated for solar to power energy conversion and have not been simulated to design an efficient PSCs. Finally, this theoretical investigation will minimize the synthetic effort for the future experimentalists.

2. Computational Methodology

Both molecular and periodic boundary condition's (PBC) simulations of the donor, acceptor, and their combinations have been carried out on Gaussian 09[26] and Quantum Espresso,[27] respectively while visualizations are achieved on *Gabedit,*[28] QuantumWise,[29] and *GaussView.*[30] Electronic structure properties of nBSD, nEDOS, and their co-oligomeric combination in the form of nEDOS-BSD (where n= 1, 2, 3…infinity) are carried out with the help of density functional theory (DFT) at hybrid functional of the B3LYP/6-31G** level of theory. The oligomeric chain length of 9BSD (**A**), 9EDOS (**D**) and 9EDOS-BSD (**D-A-D**) represent their polymeric nature very well; therefore, calculations are restricted to nine repeating units. The **D-A-D** crystal with an orthorhombic structure in the Pbcn (60) space group with 204 atoms, having lattice constants a = 4.4551 Å, b = 15.982 Å, and c = 23.91 Å are used for the PBC simulations. PBC/DFT simulations at Generalized Gradient Approximation (GGA) with a Perdew-Burke-Ernzerhof (PBE) exchange-correlation functional with a Double Zeta Polarized basis set is performed for the structural and energy optimization due to its superiority over other pseudopotentials. Monkhorst-Pack k-grid of 9x9x9 and energy cutoff of 400 eV is used in these simulations. B3LYP hybrid pseudopotential is employed for the optical properties simulations of **D-A-D**. From computational and accuracy point of view, TD-DFT is optimistic between semi-empirical and wave function approaches.[31-33] TD-DFT calculations can incorporate environmental effects and quickly give best quantitative fit to UV-vis spectra (excitation energy) of these species, especially using hybrid functionals (B3LYP).[33-35] In the case of approximate DFT, negative orbital energies (HOMO and LUMO) do not give accurate

ionization potentials (IP) and electron affinities (EA), but the deviation is about 1 eV. Since the error is method dependent and consistent for all oligomers, orbital energies can be still used to examine trends consistently.[36-48]

Furthermore, to verify our computational method, oligomeric properties of these species are extrapolated to the polymer using second order polynomial fit equations (Table S1-S3). M. Bendikov *et al* has extensively studied this group of polymers both experimentally and theoretically and confirmed the superiority of B3LYP/6-31G** level of theory over other methods.[16,49-52] Our simulated results have also a nice correlation with the experimental data as can be seen from Table S4, so, that is why the current level of theory is employed for the rest of simulations.[18,52]

Key parameters of the photovoltaic system such as reorganization energy (λ), Polaron, Bi-polaron, UV-Vis spectra, and exciton binding energy (E_b) are also simulated with the said level of theory. The stability, perturbation in electroactivity and conductivity upon mixing of donor and acceptor species are estimated from the energy of HOMO, LUMO, and band gap. The electrons and holes carrying nature are simulated from the reorganization energy and also from the contours of HOMO and LUMO, respectively. UV-vis, UV-Vis-Near IR spectra and an optical gap of the **D-A-D** are simulated, using TD-B3LYP/6-31G** level of theory.

3. Results and Discussion

3.1. *Optimized Geometries.*

Planarity in molecular geometry and the corresponding π-electrons conjugation over the backbone play an important role in the visible light absorption of a chemical substance. Optimized molecular and crystal structure of **D-A-D** are given Fig 1. An ideal 180° dihedral (Table 1) of the **D-A-D** shows that combination of donor and acceptor moieties has planarized

the geometry of the resulting polymer via establishing a delocalized π-electronic cloud density over the backbone. This intra-chain dihedral angle (180°) of the **D-A-D** is responsible for its low cost and straightforward synthetic approach. This statement is also inconsistent with the recently reported work.[16,49-52]
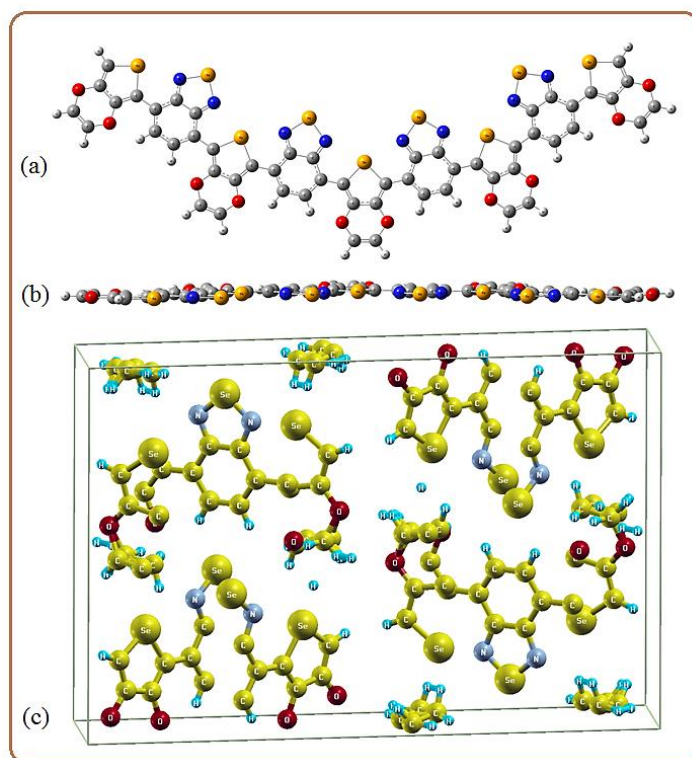

Figure 1. Optimized geometric structure of **D-A-D** (a) along with side view (b) and its Crystal Structure (c)

The dihedral angles in the intra-molecular rings of **D** are also near to planarity, however, in the case of **A** this is about 146°. The deviation in **A** from 180° is due to the internal steric hindrance of N atoms of the adjacent rings of benzo selenadiazole; caused them out of the plane as well. This out of the plane behavior of the benzo selenadiazole rings in the polymeric body may be responsible for the high resistance in delocalization of the electron cloud density (Fig 2).
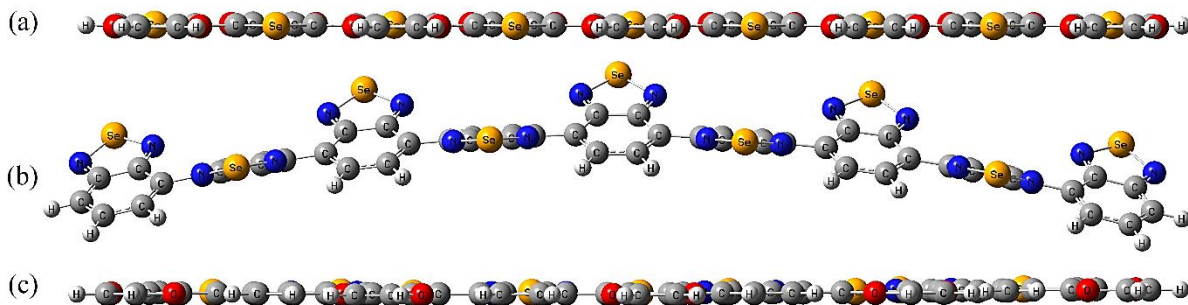
Figure 2. Optimized geometric structures of **D** (a), **A** (b) and **D-A-D** (c)

Table 1: Dihedral angles between the neighboring rings of **D**, **A**, and **D-A-D**.

#	Φ_1	Φ_2	Φ_3	Φ_4	Φ_5	Φ_6	Φ_7	Φ_8
D	179	180	179	179	179	179	180	179
A	146	148	147	149	147	149	147	148
D-A-D	180	180	180	180	180	180	180	180

3.2. Electronic Prosperities.

Charge transformation, localized and delocalized nature of the electronic cloud density of these three different oligomers are estimated from their frontier molecular orbitals, as the electronic cloud density over the HOMO predict holes and LUMO determines the possibility of the electron. The more delocalization of the charge density, higher will be the electron/hole mobility and vice versa. HOMO and LUMO of **D**, **A**, and **D-A-D** are comparatively given in Fig 3 while their orbital correlation diagram is shown in Fig 4. Molecular orbitals energy of small oligomers of these species, from monomers up to infinite chain length, are simulated and listed in Table S1-3 of the Supporting Information.
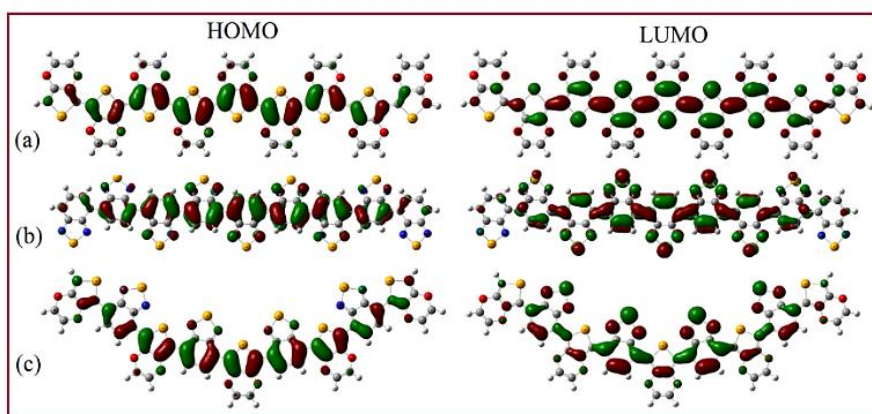
Figure 3. Contours of the HOMO and LUMO of **D** (a), **A** (b) and **D-A-D** (c)

Comparative analysis of the data of Table 2 and a visual look of the contours of HOMO and LUMO (Fig 3) predict that excited state properties in **D-A-D** are optimum compared to their individuals' **D** and **A** species. The data shown in Table 2 are specifically for the nine repeating units, however, rest of oligomeric species are given in the Supporting Information. Variation in characteristic properties is very common in short oligomers, but beyond the seven or eight repeating units, they remain almost constant. The purpose of other repeating units is to provide a range of entities which may be useful as a guideline for other experimentalists, as short oligomers are more electroactive but tricky to synthesize.
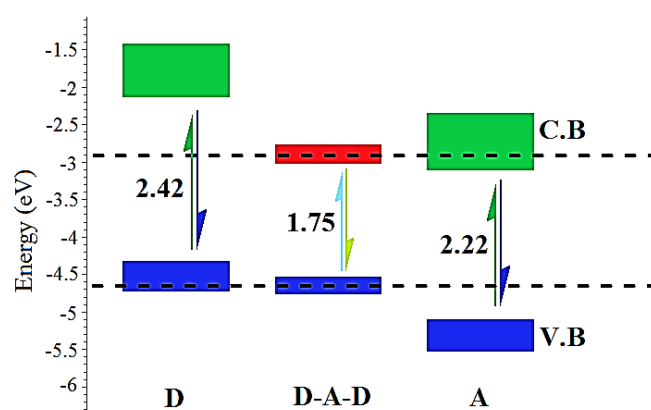

Figure 4. Orbital correlation diagram for **D**, **D-A-D**, and **A**

Our simulated HOMO, LUMO and band gap values has excellent correlation with the recently reported data.[18] Excited state properties of the different oligomers of **D-A-D**, estimated from the frontier molecular orbitals; give a clue of the free availability of π-electrons over its conjugated body (Fig. 3 and S1). These molecular orbital overlapping in the **D-A-D** (delocalized π-electrons) provides an easy pathway for the motion of free electrons which make it an excellent transparent material in the visible region of solar light (*vide infra*).

Table 2. HOMO, LUMO, Band gap, optical gap, Exciton binding and Reorganization energy in eV of the studied species at B3LYP/6-31G** level of theory.

#	HOMO	LUMO	Band gap	Optical gap	E_b	λ
D	-4.44	-2.02	2.42	2.04	0.38	0.22
A	-5.22	-2.99	2.22	1.85	0.37	0.16
D-A-D	-4.65	-2.90	1.75	1.46	0.29	0.20

The electrical band gap (estimated from the HOMO-LUMO difference) of the isolated **D** (2.42 eV) and **A** (2.22 eV) provide the evidence of their absorption in the green region of visible spectrum. Prominent near-IR absorption (red regions of the visible spectrum) by the **D-A-D** can be correlated with its band gap of 1.75 eV. Simulated band gaps of the **D**, **A**, and **D-A-D** are comparatively shown in Fig 4. The band gap reduction in all the resulted co-oligomers of **D-A-D** (Fig S3-6), highlights the importance of two opposing species in a single junction. The band structure of **D-A-D** is also obtained from the PBC simulations and has a good correlation with the molecular one, as given in Fig 5. The purpose of the PBC simulated band gap of **D-A-D** is to clarify and confirm our level of theory used.
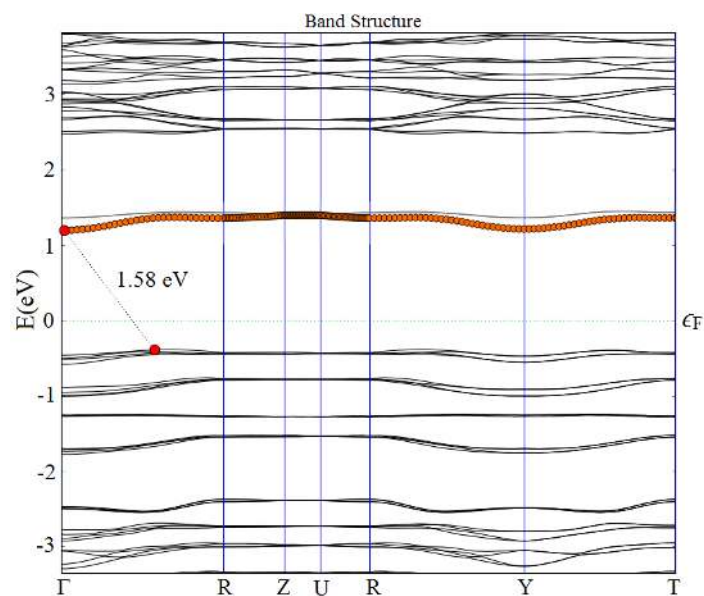
Figure 5. Band Structure of **D-A-D**

3.3. Reorganization Energy.

Reorganization energy (λ) is directly associated with the geometrical distortion of a chemical substance when it changes from neutral to cationic state. This energy is responsible for an electron to be excited from its ground state potential, charge carrier and related geometrical distortion which may be either polaron or bi-polaron. Moreover, hole mobility in an organic semiconductor can be understood in term of its reorganization energy, lower the reorganization energy the faster will be hole transformation and vice versa. The internal reorganization energies of an oligomer decrease with chain length elongation which is due to the greater positive charge (π-electrons) delocalization over the oligomeric backbone. The internal reorganization energy of **A**, **D** and **D-A-D** are simulated, using the adiabatic potential energy surface method with equation 1 (Table 2).

$$\lambda = \lambda_1 + \lambda_2 = (E_0^* - E) + (E_+^* - E_+) \qquad (1)$$

11

The E_0 and E_+ are the energies of neutral and cationic species in their lowest energy geometries and E_0^* and E_+^* represent the energy of a neutral molecule at the geometry of charged molecule and charged molecule at the geometry of the neutral molecule.

The reorganization energies of **D** is 0.22 eV which is little higher than that of **A** (0.16 eV) while that of **D-A-D** has a λ of 0.20 eV. Comparative analysis of the reorganization energies of these three different species (Table 2) led us to conclude that geometrical distortion in **A** is quite easy but on the other hand its exciton binding (0.37 eV) is higher because of its electron accepting nature. So, **D-A-D** has an optimum reorganization energy compared to the isolated **D**, and **A** but a much lower E_b (0.29 eV) which ultimately easily separate the electron-hole pair upon visible light irradiation. Moreover, we also compared our simulated λ to the already reported hole transporting organic semiconducting materials.[53,54] These hole transporting materials such as *N,N′*-diphenyl-*N,N′*-bis(3-methylphenyl)-(1,1′-biphenyl)-4,4′-diamine has 0.33 eV,[55] ((*N,N′*-bis(2,4-dimethyl-phenyl)-*N*-(4′-((2,4-dimethylphenyl) (phenyl)amino)-[1,1′-bi-phenyl]-4-yl)-*N′*-phenyl-[1,1′-biphenyl]-4,4′-diamine has 0.23 eV, 4-(4-phenyl-4-*α*-naphthylbutadienyl)-*N,N*-di(4-tolyl)-phenylamine has 0.24[53] and silole-based organic semiconductors has 0.50 eV[54] internal reorganization energy. So, it is verified that **D-A-D** has better hole transferability due to lower reorganization energy which may be correlated to its fully planner geometrical structure with an ideal dihedral of 180°.

3.4. *Polaron, Bi-polaron, and Exciton Binding Energy.*

It is generally believed that PSCs require well-controlled movement of charges for efficient photon conversion.[56] In conjugated polymers, usually polaronic and bi-polaronic states appear within the parent band gap[57] upon doping with appropriate doping agents. These are the key tools for charge storage and charge transportation in COPs. Charge and the associated distortion along the backbone of COP create either polaron or bi-polaron. Single charge and

the associated distortion are termed as polaron (delocalized state), denoted as E_p while a pair of charges and their distortion in the polymeric body is regarded as bi-polaron. Bi-polarons states are comparatively stable, localized and less electroactive to that of polarons. Donation of charge by a particular conjugated system is followed by intra-molecular relaxation which can be precisely called as polaronic effect. Polaron-binding energy can be easily obtained from the reorganization energy (λ) using an expression such as $E_p = (1/2\,\lambda)$. On the other hand, exciton binding energy or an electron−hole binding energy is the amount of that barrier (coulombic energy) with which the lowest unoccupied orbital accepts an extra electron and left behind the occupied orbital as degenerate. We have simulated the exciton binding energy (E_b) from the energy difference of neutral exciton and the two free charge carriers, using an expression such as $E_b = E_{\text{Band gap}} - E_{\text{Optical gap}}$.

Molecular orbital energy diagram of the neutral, cationic and di-cationic states of **D** is depicted in Fig 6, where orbital transition along with energy is clearly shown. Band gap and exciton binding energy of **D** in its neutral state are 2.42 and 0.38 eV, respectively. Mono-cationic state in the unrestricted formalism and in the absence of counter-ion is considered to efficiently explore the polaronic effect. Removal of an electron from the oligomeric backbone of **D** induces an extra band within its parental band gap, regarded as inter-band. Mono-cationic state not only reduces the band gap (2.23 or 2.15 eV) of parent **D** by lowering down the HOMO and LUMO energy levels but also increases the delocalization over the polymeric backbone (Fig S7). The delocalization over the oligomeric body of mono-cationic state can be seen from the non-degenerate molecular orbitals, termed as Alpha and Beta (Fig 6) or polaron. However, restricted and unrestricted formalisms of the Kohn-Sham orbitals have a similar effect on the molecular orbital distribution of di-cationic state in **D**. Di-cationic state of **D**, creates a bi-polaronic state as can be seen from its degenerate frontier molecular orbitals (Fig 6). This

degenerate state in the highly cationic state is not only responsible for reducing the band gap but promotes stability compared to that of the polaronic state.
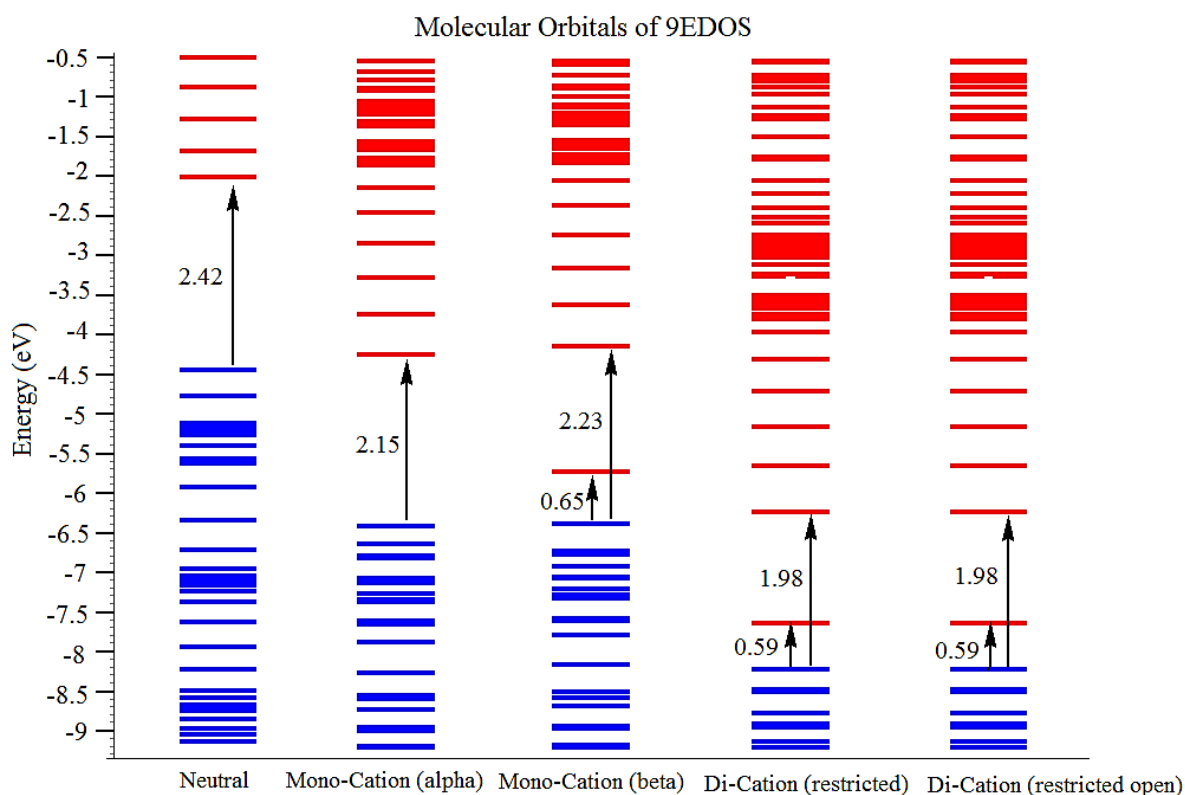

Figure 6. Energy level diagram of the neutral, mono, and di-cationic state of **D**.

A similar trend in the molecular orbital distribution of **A** is observed upon making its cationic and di-cationic states, as shown in Fig 7. Band gap of the acceptor species in the neutral state is found to be 2.22 eV while the coulombic force which holds the electron-hole pair is 0.37 eV. The frontier molecular orbital cloud densities of the neutral, cationic and di-cationic states are given in Fig S8 of the Supporting Information.
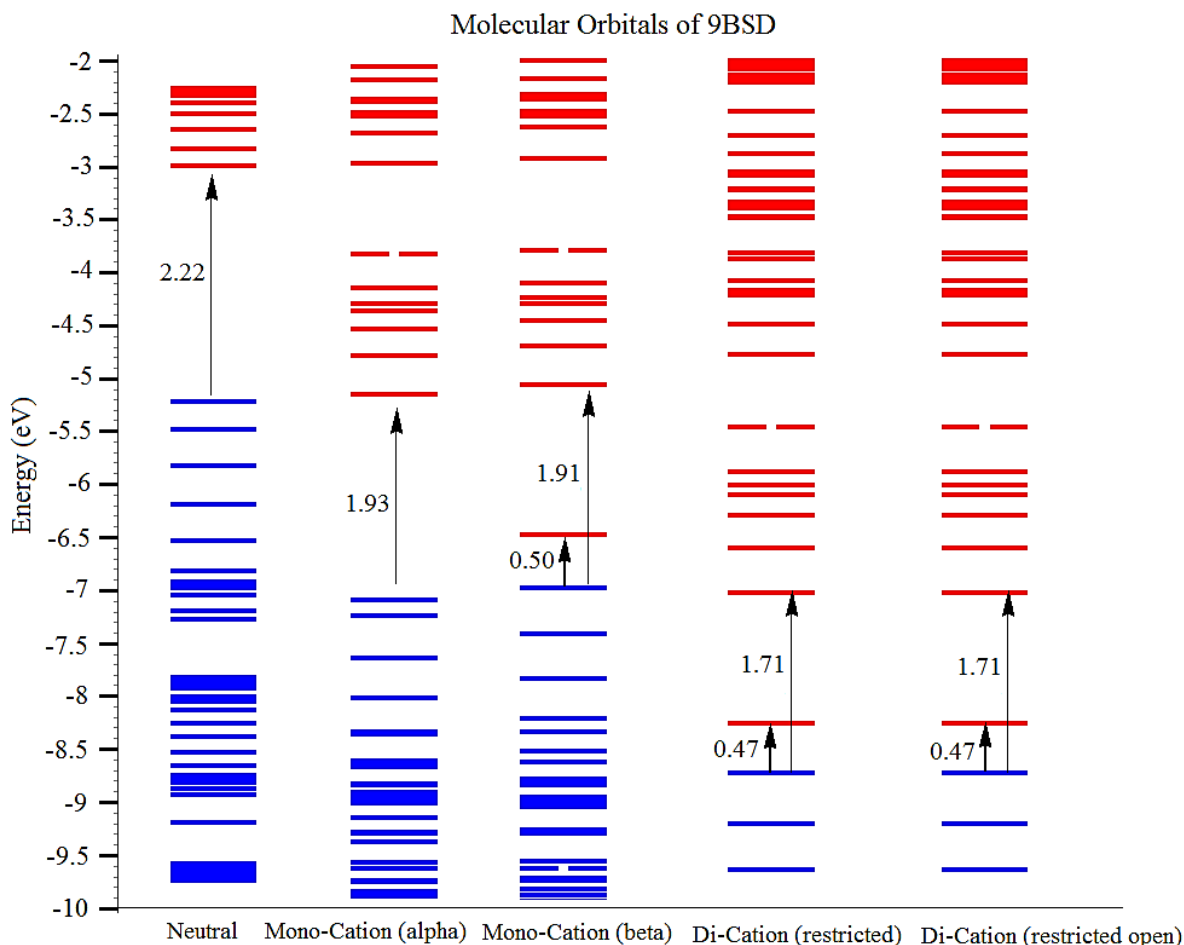
Figure 7. Energy level diagram of the neutral, mono, and di-cationic state of **A**.

The combination of the **D** and **A** moieties in the oligomeric form such as **D-A-D** has much stretched down the HOMO and LUMO energy levels which result in a band gap of 1.75 eV. Analysis of the contours of HOMO and LUMO (Fig S9) of **D-A-D** reflect an evidence of strong overlapping of the **D** and **A** orbitals. Keeping in mind the exciton binding energies of **D** and **A**, this donor-acceptor combination has considerably lowered down the E_b (0.29 eV). So, this lower exciton binding energy and narrow band gap are clear indications for the charge separation (electron-hole pair) at the donor-acceptor interface (here acceptor is the PCBM in the PSC device) and high short-circuit current density, respectively (*vide infra*).
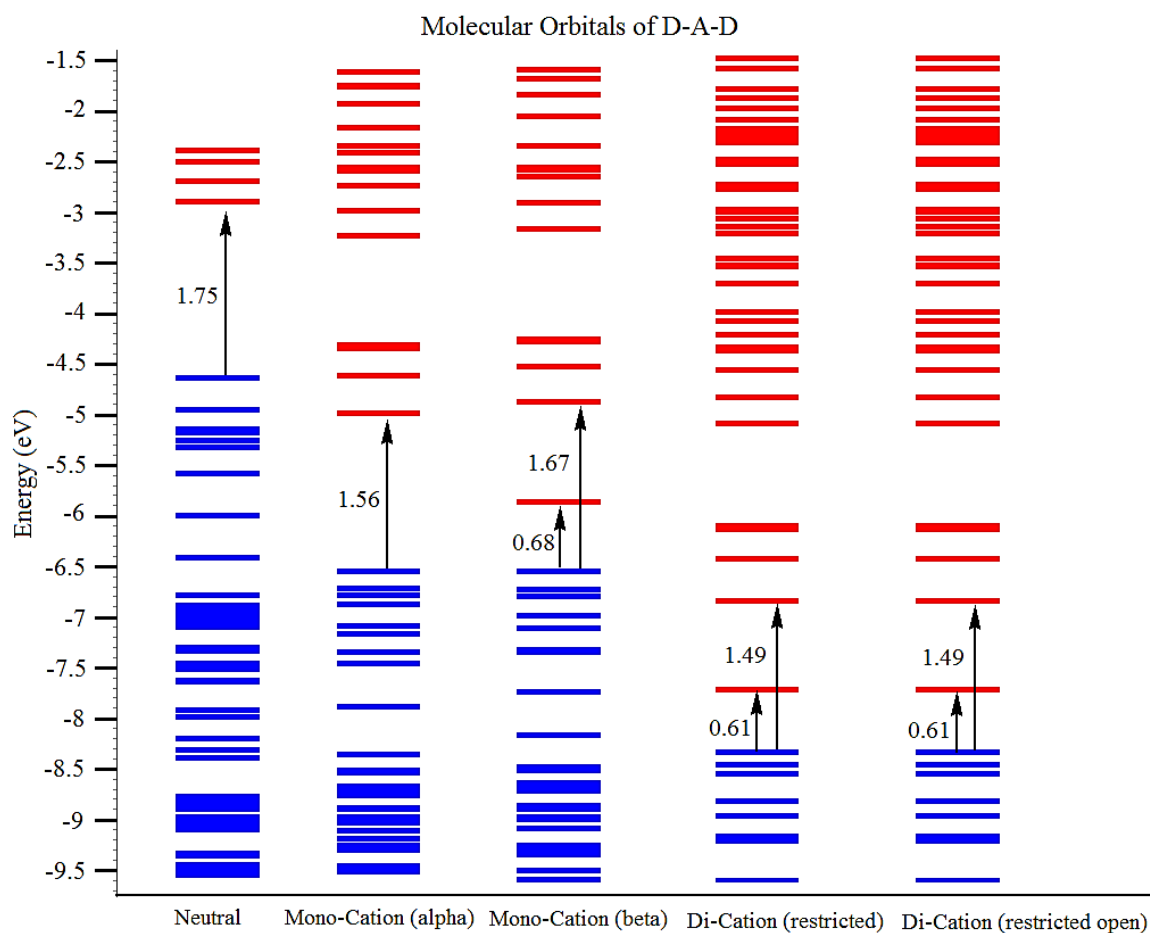
Figure 8. Energy level diagram of the neutral, mono, and di-cationic state of **D-A-D.**

The simulated narrow band gap (1.75 eV) of the **D-A-D** has a good correlation with the experiment, which strongly validates the level of theory, we used.[18] To further validate the electronic properties of the designed polymer, cationic and di-cationic states are considered, upon removal of one and two electrons in the absence of counter ions, respectively. Oxidation causes a reduction in the band gap from 1.75 to 1.56 eV (considering the Alpha orbitals) and 1.75 to 1.67 eV on considering the Beta orbital distributions. As explained earlier, a cation along with associated distortion produces a non-degenerate state; polaron (Fig 8). On further oxidation of the **D-A-D** species (extraction of a pair of electrons) in the absence of counter ions, result in a bi-polaronic state over the π-conjugated backbone which further reduces the orbitals band gap to 1.49 eV. The bi-polaronic state creates an extra band, called inter-band

transition which arises from the σ→π* orbital transition and has an energy of 0.61 eV. As explained earlier, the stability of bi-polaron over the polaron is due to these degenerate molecular orbitals. Moreover, restricted and unrestricted formalism has a similar effect in the di-cationic states.

3.5. *UV-Vis and UV-Vis-Near-IR Absorption Spectral Analysis*

UV-Vis and UV-Vis-Near-IR absorption spectra of the **D**, **A**, and **D-A-D** along with their corresponding mono and di-cationic states are simulated at TD-DFT. Generally, light absorption by conjugated polymers causes single and strong absorption in the visible region where an electron transferred from HOMO to LUMO. Moreover, this absorption band peak red-shifts with chain length elongation of the conjugated body.[58,59] Absorption spectra of all these three species along with their defective states are categorized into separate sections.

Mostly COPs are positively charged when experimentally synthesized so, that is why the cationic and di-cationic states are considered to efficiently explore the solar light absorption abilities. The UV-Vis spectra of the neutral state of **D** (Fig 9) show two distinct peaks at ca. 608 and 440 nm and arises from $\pi \rightarrow \pi^*$ and HOMO-1 to LUMO-1 transition, respectively. The effect of cationic and di-cationic is investigated in the absence of counter-ion; where the mono-cation induces polaron and deficiency of two electrons create a bi-polaron state.
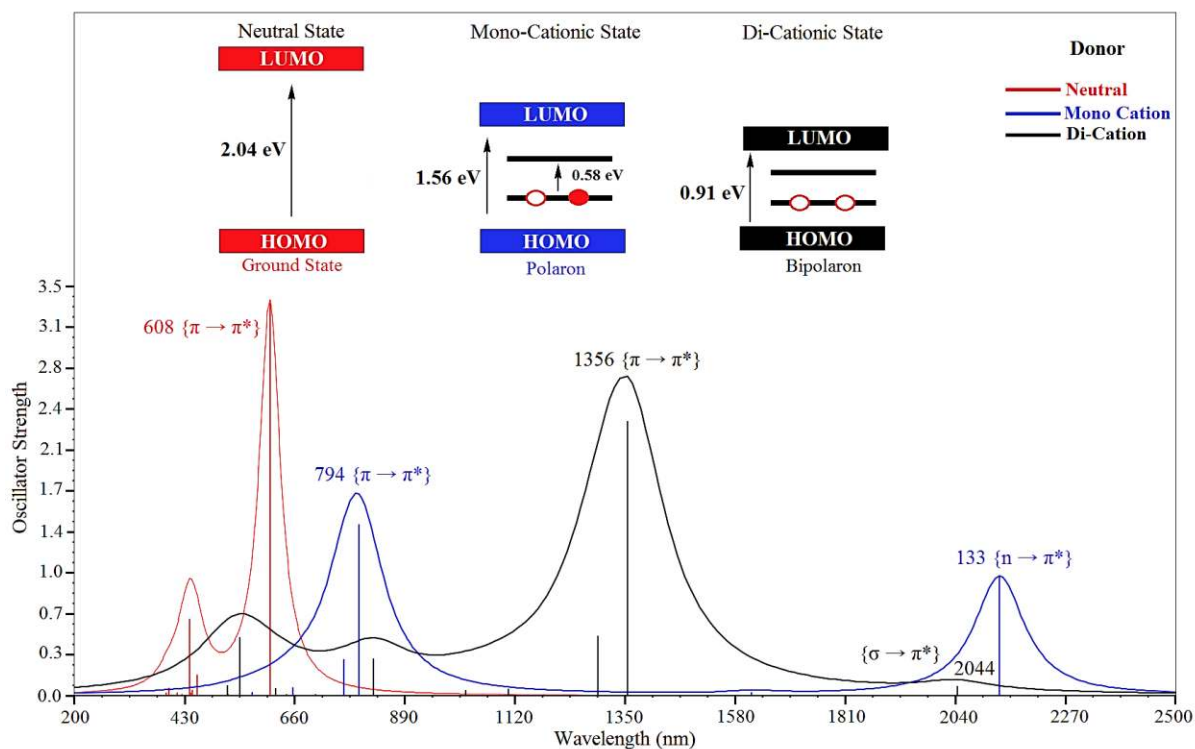
Figure 9. UV-vis Spectra along with Optical band gaps of Neutral, Mono, and Di-Cationic states of **D** at B3LYP/6-31G**.

Upon removal of an electron from the oligomeric backbone of **D**, creates an extra absorption peak in the Near-IR region at ca. 2133 nm. Compared to the parent **D**, a red-shifting of about 186 nm in the λ_{max} is achieved in its cationic state. The lower energy absorption peak at a longer wavelength (2133 nm) is because of the delocalized polaronic state which is simply due to $\sigma \rightarrow \pi^*$ transition or inter-band transition. This longer wavelength absorption, near the IR region, is responsible for the delocalized electronic cloud density over the oligomeric chain length (*vide supra*). From the UV-Vis-Near-IR spectra, we can see that mono-cationic state may be much efficient for the solar spectrum absorption but unstable compared to the ground state.

Creation of a di-cationic state in **D**, significantly red-shifts the λ_{max} from 608 to 1356 nm and give rise to a weak $\sigma \rightarrow \pi^*$ transition (2044 nm) within the parent optical band gap. The lower

excitation energy of the $\pi \rightarrow \pi^*$ in the bi-polaronic state is a direct consequence of its stability and localized nature compared to that of the polaronic state. The reduced optical band gap of the di-cationic state has a wide range absorption of Near-IR radiation besides visible spectrum of light. So, both of these polaron and bi-polaron states can be easily induced in the polymeric body to enhance the visible light absorption in the PSC device, upon covalent and non-covalent doping. In summary, a well-doped state of the **D** can also give desirable efficiency if used in the BHJ of the PSC (*vide supra*).

UV-Vis spectra of **A** give rise to a strong absorption band peak which is peaked at 669 nm and is termed as the first allowed $\pi \rightarrow \pi^*$ transition, capable of red light absorption of the solar spectrum, shown in Fig 10. In the polaronic state (mono-cationic), a significant amount of red-shifting in absorption is simulated in the λ_{max} (669 to 969 nm) and generate an inter-band transition. This inter-band peak arises from the transition of the partially occupied (n) molecular orbital to the vacant conduction (π^*) band state. This forbidden absorption band peak is situated at 2430 nm and consequences a high delocalized π-electronic cloud density over the oligomeric body. The $n \rightarrow \pi^*$ transition in higher wavelength region is because of the absence of counter-ion, which creates high electroactivity and instability. This polaronic trend in **A** is almost similar to that of **D** but substantially pronounced. Removal of two electrons from the oligomeric chain length of **A** establishes a stable and much prominent bi-polaronic state compared to **D**. The first allowed $\pi \rightarrow \pi^*$ transition in **A** spans in the range of 1513 nm, which is capable of absorbing both the visible and Near-IR radiations of the solar spectrum. Furthermore, this localized di-cationic state along with associated distortion provide an easy pathway for the electron/hole transformation along the π-conjugated backbone (*vide supra*). The bi-polaronic state has wide range absorption of the solar spectrum as can be seen from the broad and high-intensity band peak at ca. 1513 nm.
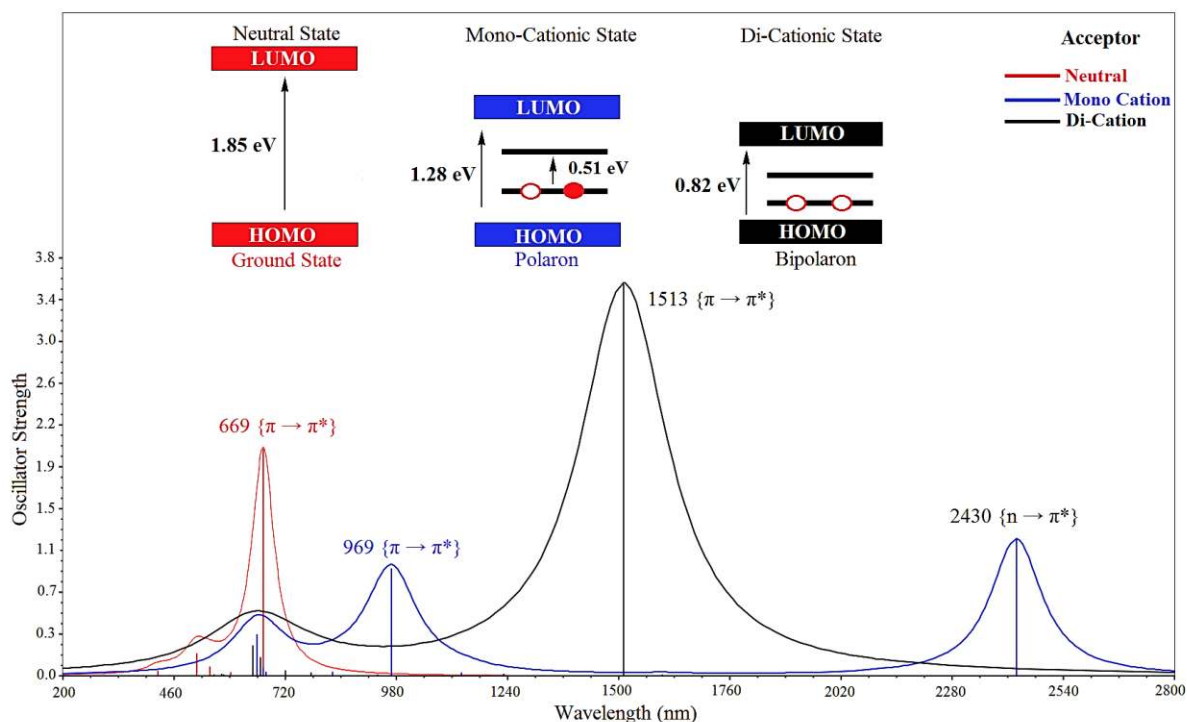
Figure 10. UV-Vis Spectra along with Optical band gaps of the Neutral, Mono, and Di-Cationic states of **A** at B3LYP/6-31G**.

Comparative UV-Vis spectra of **D**, **A**, and **D-A-D** are given in Figure 11, where the maximum absorption band peaks are peaked at 608, 669 and 847 nm, respectively. These bands can also be regarded as the first allowed maximum electronic excitation (the one with higher oscillator strength) in the visible region and are due to $\pi \rightarrow \pi^*$ transitions (Table 3). The absorption band peak at ca. 847 nm in **D-A-D** is a strong evidence of its efficient absorption in the visible region and responsible for charge transferring ability as well. Moreover, this simulated λ_{max} has a strong correlation with the already experimental observed UV-Vis spectra (843 nm)[18] which also supports and confirmed the level of theory used (See Fig S10 of the Supporting Information). Furthermore, it can be concluded that this wide range of the visible light absorption in the **D-A-D** is responsible for higher efficiency, compared to that of their individual counterparts. From Fig 11, it is evident that how the Donor and Acceptor moieties in the form of **D-A-D**, increase the visible light absorption in a particular polymer.
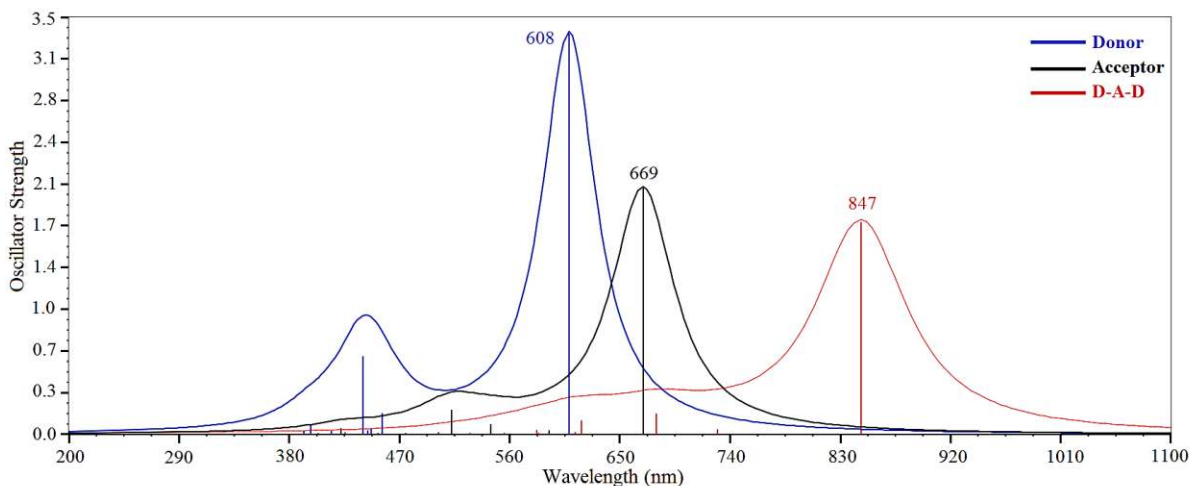
Figure 11. UV-vis Spectra of **A**, **D**, and **D-A-D** at B3LYP/6-31G**.

As discussed above, a reduction in the optical band gap of the resulted polymer along with wide UV-Vis absorption is achieved through a mutual overlapping of the molecular orbitals of donor and acceptor. The UV-vis spectra of **D-A-D** has three distinct absorptions; two small peaks in the visible and a broad one near the IR region, which is an indication of its efficient light-harvesting ability. Furthermore, we also predicted the polaron and bi-polaron states in the extended conjugation of **D-A-D**, which is given in Figure 12.

Table 3: First three vertical allowed transitions along with *f* and MO transition.

Species	*Excited Energy (eV)*	*λ (nm)*	*f*	*Electronic Transition*
D	1	608	3.35	HOMO→LUMO
	2	456	0.17	HOMO$_{-3}$→LUMO
	3	440	0.65	HOMO$_{-1}$→LUMO$_1$
A	1	669	2.06	HOMO→LUMO
	2	544	0.08	HOMO→LUMO$_2$
	3	512	0.20	HOMO$_{-1}$→LUMO$_1$
D-A-D	1	847	1.78	HOMO→LUMO

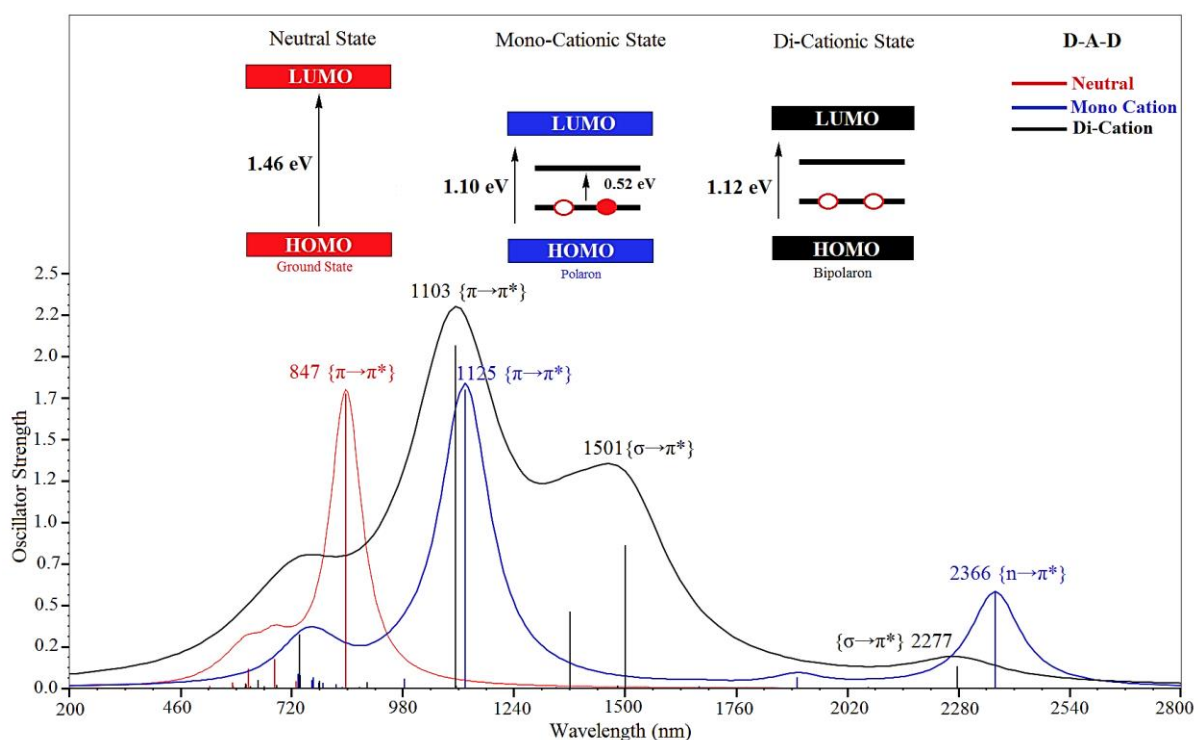|			
2	680	0.17	HOMO$_{-1}\rightarrow$LUMO
3	618	0.12	HOMO$_{-1}\rightarrow$LUMO$_1$

Figure 12. UV-Vis Spectra along with Optical band gaps of Neutral, Mono, and Di-Cationic states of **D-A-D** at B3LYP/6-31G**.

Once again, a similar trend is observed in the case of **D-A-D**, upon creation of polaronic and bi-polaronic states. Optical band gap of the parent **D-A-D** is 1.46 eV, which reduces to 1.10 eV in the mono-cationic state. The optical band gap of the bi-polaronic state is about 1.12 eV which is because of the $\pi\rightarrow\pi^*$ transition. Unlike the **D**, and **A**, UV-Vis-Near-IR spectra of the di-cationic state is ideal and transparent in the whole region of the solar spectrum. Additionally, two extra low energy band peaks, located at 1501 and 2277 nm strengthen the absorption ability

of **D-A-D** in the bi-polaronic state. These near-IR absorptions arise from the electronic transition of σ→π* orbitals.

3.6. *Theoretical Performance of Polymer Solar Cells.*

To get the high efficiency of bulk heterojunction (BHJ) polymer solar cell, scientists are struggling to achieve higher (i) short-circuit current density (J_{sc}) (ii) open circuit voltage (V_{oc}) (iii) and a high fill factor (FF). The efficiency of a PSC can be obtained using equation 2,[4]

$$\eta = \frac{V_{oc} \times J_{sc} \times FF}{P_{in}} \times 100 \qquad (2)$$

where η is efficiency and P_{in} is the power density of incident light.

The J_{sc} has an inverse relation with the band gap value in PSC; lower the band gap much higher will be the short-circuit current density and vice versa. So, narrow band gap polymer can harvest sufficient amount of sunlight and lead to enhanced J_{sc}. Furthermore, J_{sc} is also dependent on the LUMO energy levels of the hole transporting material (here **D-A-D**) and acceptor (PCBM) in the PSC device. If the difference is more than 0.3 eV (equation 3), then the device will result in high J_{sc}, and this energy difference can also be correlated with charge transport (η_{cT}) within PSC. The smaller-scale phase separation creates larger area of interfaces where charge separation can take place. A large energy difference between the LUMO of **D-A-D** (donor) and the LUMO of PCBM (acceptor) is required for ultrafast photoinduced electron transfer.[60] The next important parameter of the PSC is the V_{oc}, which can be tuned/enhanced by lowering down the HOMO level of the polymer in the BHJ. Theoretically, the V_{oc} of PSCs can be estimated from the orbital difference of **D-A-D** (HOMO) and PCBM (LUMO), using equation 3.[4]

$$V_{oc} = e^{-1} \times (|E_{HOMO}Donor| - |E_{LUMO}Acceptor| - 0.3eV \qquad (3)$$

Where e⁻ is the elementary charge, E is the energy level and 0.3 eV is an empirical value for efficient charge separation (minimum difference of the LUMOs of donor and acceptor). The final crucial parameter in getting the high efficiency of PSC is the FF, which is simply a ratio between the maximum obtainable power and the product of V_{oc} and J_{sc}. FF is strongly dependent on the film morphology, interface recombination, miscibility of polymer and PCBM and high charge carrier mobility in the PSC. So, from a molecular point of view, a planner polymer with high delocalized π-electrons, molecular chain packing, and good crystallinity are prime factors for high FF.
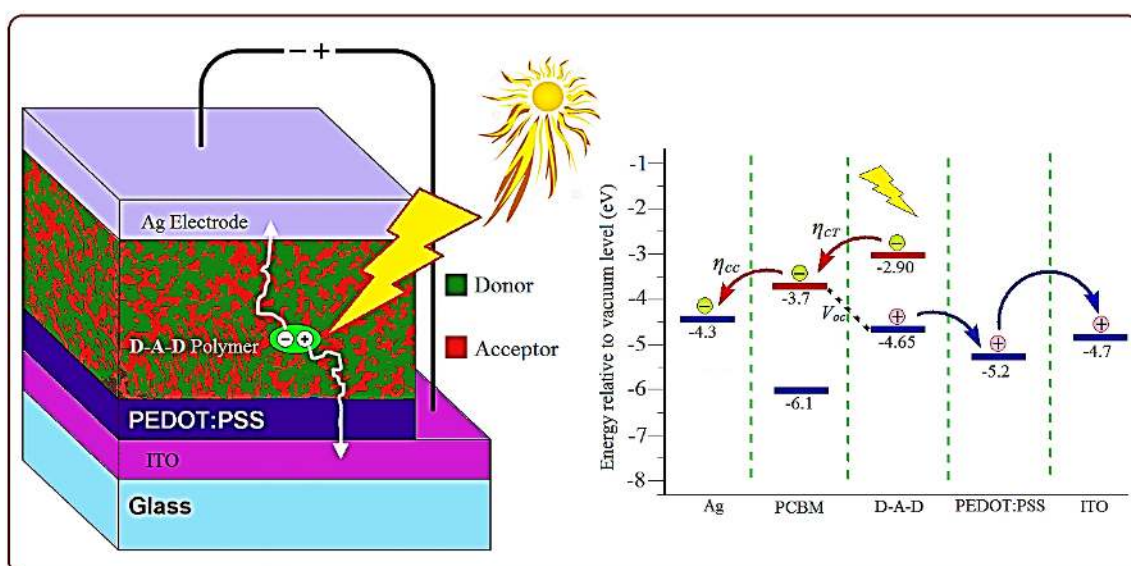

Figure 13. Supposed device structure of the inverted organic solar cell along with energy band diagram of **D-A-D** and other species.

Theoretical performance of our investigated **D-A-D** is finally modeled for the solar cell application in a BHJ structure which is schematically given in Fig 13. The photovoltaic properties of **D-A-D** are modeled in a device structure of ITO|PEDOT:PSS/**D-A-D**:PCBM|Ag; where ITO, indium tin oxide; PEDOT:PSS, poly(styrene sulfonate)-doped poly(ethylene-dioxythiophene); PCBM, and other fullerenes derivatives. Theoretical open circuit voltage (*Voc*) and the corresponding LUMO-LUMO difference of **D-A-D** and PCBM derivatives are

24

correlated with J_{sc} and charge transport energy (η_{cT}), respectively. All other parameters of the device are taken from experimental work such as illumination of AM 1.5G, weight ratios of **D-A-D** and PCBM (fullerene derivatives) were 1:1.[61]

Table 4. HOMO, LUMO of fullerene derivatives and open circuit voltage (V_{oc}) and LUMO^{Donor}—LUMO^{Acceptor} energy difference (L-L) of **D-A-D**; all values are in eV.

#	Species	HOMO	LUMO	V_{oc}	L-L
1	PC$_{61}$BM[62]	-6.10	-3.63	1.02	0.73
2	PC$_{61}$BM[63]	-6.10	-3.70	0.95	0.80
3	IC$_{60}$BA[64]	-5.80	-3.70	0.95	0.80
4	IC$_{60}$BA[65]	-5.85	-3.74	0.91	0.84
5	IC$_{60}$MA[65]	-5.91	-3.86	0.79	0.90
6	PC$_{60}$BM[66]	-5.93	-3.91	0.74	1.01
7	PC$_{70}$BM[67]	-5.87	-3.91	0.74	1.01
8	PC$_{70}$BM[68]	-6.0	-4.0	0.65	1.10
9	PC$_{71}$BM[64]	-6.0	-4.0	0.65	1.10
10	PC$_{61}$BM[69]	-6.2	-4.10	0.55	1.20

The photovoltaic properties of **D-A-D** in the PSC device such as *Voc* and charge transport are simulated which are listed in Table 4. Different HOMO and LUMO energy levels of the fullerenes derivatives are reported (Table 4), however, few of them are considered with our investigated **D-A-D** polymer. From Table 4, it can be analyzed that the *Voc* of the PSC has a direct relation with the LUMO energy level of PCBM, higher the LUMO level results in large *Voc*. A PC$_{61}$BM[62] with LUMO energy level of -3.63 eV, produces *Voc* of 1.02 eV with our designed **D-A-D**, however, this voltage drops down to 0.65 eV when PC$_{71}$BM[64] is used (LUMO, -4.0 eV). Comparative analysis of the data of Table 4 led us to predict that an average

open circuit voltage of roundabout 0.90 eV can be achieved, using **D-A-D** as donor material in the BHJ solar cell devices. Compared to individual **D** and **A** conformer, the resulted constituent has planner geometry so, a high FF is expected and the narrow optical band gap (1.46 eV) and electrical band gap (1.75 eV) are responsible for high *Jsc* (*vide supra*).

Conclusion

Solar to power energy conversion via photovoltaic process is a clean and renewable energy technology which holds a sustainable development. We have used density functional theory (DFT) and time-dependent (TD-DFT) at hybrid functional, to assess the nature and electronic properties of a near-infrared-absorbing, low energy gap conjugated polymer; donor−acceptor−donor (**D-A-D**). The **D-A-D** is consisting of *2,1,3*-benzosele-nadiazole (**A**) as acceptor and *3,4*-ethylenedioxyselenophene (**D**) as donor fragments. The **D** and **A** moieties in the polymeric backbone have been found to be responsible for reducing the band gap, open circuit (*Voc*) and increasing short-circuit current density (*Jsc*) in polymers solar cells (PSC). Our theoretical studies revealed that charge transportation efficiency (η_{CT}), *Voc*, *Jsc* and, in turn, device performance, are influenced by electronic energy level alignment at interfaces. A lower HOMO energy level (-4.65 eV) of designed **D-A-D** is responsible for increasing the ambient stability during device operation and results in high *Voc* of 1.02 eV. Furthermore, it is found that donor-acceptor combination has a key role in charge separation, weak steric hindrance, and molecular architecture (planarity of the polymeric backbone) which directly influences the charge transport compared to that of counterpart homopolymers (either **D** or **A**). Reduction in the band gap, high charge transformation, and enhanced visible light absorption in **D-A-D** system is because of strong overlapping of the frontier molecular orbitals of the **D** and **A**. A highly energetic, unstable and delocalized polaronic state exists when the polymer was oxidized (cationic state) while further oxidation (di-cationic state) generates a

26

comparatively stable and localized state, bi-polaron. Finally, these polaron and bi-polaron are found to have a direct relation with visible light absorbed photocurrent generation.

Supporting Information

Tables for the values of the valence band, conduction band, and band gaps of **D**, **A** and **D-A-D** from monomer up to infinite chain length. Figures of the band development upon chain length elongation, molecular orbital contours and absorption spectra of **D**, **A** and **D-A-D.** This material is available free of charge via the Internet at http://pubs.acs.org.

Corresponding Authors

Habib Ullah

Email: habib_chemist@yahoo.com; hu203@exeter.ac.uk

Asif Ali Tahir

Email: A.Tahir@exeter.ac.uk

Notes

The authors declare no competing financial interest.

References

(1) Wolf, J.; Babics, M.; Wang, K.; Saleem, Q.; Liang, R. Z.; Hansen, M. R.; Beaujuge, P. M. Benzo[1,2-b:4,5-b']Dithiophene-Pyrido[3,4-b]Pyrazine Small-Molecule Donors for Bulk Heterojunction Solar Cells. *Chem. of Mater.* **2016**, *28*, 2058-2066.

(2) Wang, M.; Cai, D.; Yin, Z.; Chen, S. C.; Du, C. F.; Zheng, Q. Asymmetric-Indenothiophene-Based Copolymers for Bulk Heterojunction Solar Cells with 9.14% Efficiency. *Adv. Mater.* **2016**, *28*, 3359-3365.

(3) Scharber, M.; Sariciftci, N. Efficiency of Bulk-Heterojunction Organic Solar Cells. *Prog. Polym. Sci.* **2013**, *38*, 1929-1940.

(4) Li, G.; Zhu, R.; Yang, Y. Polymer Solar Cells. *Nat. Photon.* **2012**, *6*, 153-161.

(5) Green, M. A.; Emery, K.; Hishikawa, Y.; Warta, W.; Dunlop, E. D. Solar Cell Efficiency Tables (Version 45). *Prog. Photovoltaics Res. Appl.* **2015**, *23*, 1-9.

(6) Scharber, M. C.; Mühlbacher, D.; Koppe, M.; Denk, P.; Waldauf, C.; Heeger, A. J.; Brabec, C. J. Design Rules for Donors in Bulk-Heterojunction Solar Cells—Towards 10% Energy-Conversion Efficiency. *Adv. Mater.* **2006**, *18*, 789-794.

(7) Heeger, A. J. Semiconducting and Metallic Polymers: The Fourth Generation of Polymeric Materials (Nobel Lecture). *Angew. Chem. Inter. Ed.* **2001**, *40*, 2591-2611.

(8) Heeger, A. J. Semiconducting and Metallic Polymers: The Fourth Generation of Polymeric Materials. *J. Phys. Chem. B* **2001**, *105*, 8475-8491.

(9) Facchetti, A. π-Conjugated Polymers for Organic Electronics and Photovoltaic Cell Applications. *Chem. Mater.* **2010**, *23*, 733-758.

(10) Ullah, H.; Tahir, A. A.; Mallick, T. K. Polypyrrole/TiO_2 Composites for the Application of Photocatalysis. *Sens. Actuators, B* **2016**.

(11) Ullah, H. Inter-Molecular Interaction in Polypyrrole/TiO_2: A DFT Study. *J. Alloys Compd.* **2017**, *692*, 140-148.

(12) Salzner, U. Quantitatively Correct UV-Vis Spectrum of Ferrocene with TD-B3LYP. *J. Chem. Theo. Comput.* **2013**, *9*, 4064-4073.

(13) Mikhnenko, O. V.; Azimi, H.; Scharber, M.; Morana, M.; Blom, P. W.; Loi, M. A. Exciton Diffusion Length in Narrow Bandgap Polymers. *Energy Environ. Sci.* **2012**, *5*, 6960-6965.

(14) Müllen, K.; Pisula, W. Donor–Acceptor Polymers. *J. Am. Chem. Soc.* **2015**, *137*, 9503-9505.

(15) Scharber, M. C. On the Efficiency Limit of Conjugated Polymer: Fullerene-Based Bulk Heterojunction Solar Cells. *Adv. Mater.* **2016**, *28*, 1994-2001.

(16) Tan, H.; Furlan, A.; Li, W.; Arapov, K.; Santbergen, R.; Wienk, M. M.; Zeman, M.; Smets, A. H.; Janssen, R. A. Highly Efficient Hybrid Polymer and Amorphous Silicon Multijunction Solar Cells with Effective Optical Management. *Adv. Mater.* **2016**, *28*, 2170-2177.

(17) Brédas, J.-L.; Norton, J. E.; Cornil, J.; Coropceanu, V. Molecular Understanding of Organic Solar Cells: The Challenges. *Acc. Chem. Res.* **2009**, *42*, 1691-1699.

(18) Poverenov, E.; Zamoshchik, N.; Patra, A.; Ridelman, Y.; Bendikov, M. Unusual Doping of Donor–Acceptor-Type Conjugated Polymers Using Lewis Acids. *J. Am. Chem. Soc.* **2014**, *136*, 5138-5149.

(19) Wang, D. H.; Kim, D. Y.; Choi, K. W.; Seo, J. H.; Im, S. H.; Park, J. H.; Park, O. O.; Heeger, A. J. Enhancement of Donor–Acceptor Polymer Bulk Heterojunction Solar Cell Power Conversion Efficiencies by Addition of Au Nanoparticles. *Angew. Chem.* **2011**, *123*, 5633-5637.

(20) Alam, M. M.; Jenekhe, S. A. Efficient Solar Cells from Layered Nanostructures of Donor and Acceptor Conjugated Polymers. *Chem. Mater.* **2004**, *16*, 4647-4656.

(21) Kim, K.; Liu, J.; Namboothiry, M. A.; Carroll, D. L. Roles of Donor and Acceptor Nanodomains in 6% Efficient Thermally Annealed Polymer Photovoltaics. *Appl. Phys. Lett.* **2007**, *90*, 163511.

(22) Yu, G.; Gao, J.; Hummelen, J. C.; Wudl, F.; Heeger, A. J. Polymer Photovoltiac Cells: Enhanced Efficiencies Via a Network of Internal Donor-Acceptor Heterojunctions. *Science* **1995**, *270*, 1789.

(23) Benten, H.; Mori, D.; Ohkita, H.; Ito, S. Recent Research Progress of Polymer Donor/Polymer Acceptor Blend Solar Cells. *J. Mater. Chem. A* **2016**, *4*, 5340-5365.

(24) Ogawa, Y.; White, M. S.; Sun, L.; Scharber, M. C.; Sariciftci, N. S.; Yoshida, T. Substrate-Oriented Nanorod Scaffolds in Polymer–Fullerene Bulk Heterojunction Solar Cells. *Chem. Phys. Chem.* **2014**, *15*, 1070-1075.

(25) Kim, S.-O.; Kim, Y.-S.; Yun, H.-J.; Kang, I.; Yoon, Y.; Shin, N.; Son, H. J.; Kim, H.; Ko, M. J.; Kim, B. N-Octyl-2, 7-Dithia-5-Azacyclopenta [a] Pentalene-4, 6-Dione-Based Low Band Gap Polymers for Efficient Solar Cells. *Macromolecules* **2013**, *46*, 3861-3869.

(26) Frisch, M. J. T. G. W.; Schlegel, H. B.; Scuseria, G. E.; Robb, M. A.; Cheeseman, J. R.; Scalmani, G.; Barone, V.; Mennucci, B.; Petersson, G. A.; et al. *Gaussian 09*, Rev. D. 0.1; Gaussian, Inc.: Wallingford, CT, 2013

(27) Giannozzi, P.; Baroni, S.; Bonini, N.; Calandra, M.; Car, R.; Cavazzoni, C.; Ceresoli, D.; Chiarotti, G. L.; Cococcioni, M.; Dabo, I. Quantum Espresso: A Modular and Open-Source Software Project for Quantum Simulations of Materials. *J. Phys.: Condens. Matter* **2009**, *21*, 395502.

(28) Allouche, A. R. Gabedit–A Graphical user Interface for Computational Chemistry Softwares. *J. Comput. Chem.* **2011**, *32*, 174−182.

(29) Virtual NanoLab Version 2016.2, QuantumWise A/S (www.quantumwise.com)

(30) Dennington, R. D.; Keith, T. A.; Millam, J. M. Gaussview 5.0,8. Gaussian Inc.: Wallingford, CT, 2008.

(31) Jacquemin, D.; Wathelet, V.; Perpete, E. A.; Adamo, C. Extensive TD-DFT Benchmark: Singlet-Excited States of Organic Molecules. *J. Chem. Theo. Comput.* **2009**, *5*, 2420-2435.

(32) Cramariuc, O.; Hukka, T. I.; Rantala, T. T.; Lemmetyinen, H. TD-DFT Description of Photoabsorption and Electron Transfer in a Covalently Bonded Porphyrin-Fullerene Dyad. *J. Phys. Chem. A* **2006**, *110*, 12470-12476.

(33) Sun, H.; Autschbach, J. Electronic Energy Gaps for Π-Conjugated Oligomers and Polymers Calculated with Density Functional Theory. *J. Chem. Theo. Comput.* **2014**, *10*, 1035-1047.

(34) Jacquemin, D.; Perpete, E. A.; Scuseria, G. E.; Ciofini, I.; Adamo, C. TD-DFT Performance for the Visible Absorption Spectra of Organic Dyes: Conventional Versus Long-Range Hybrids. *J. Chem. Theo. Comput.* **2008**, *4*, 123-135.

(35) Berardo, E.; Hu, H.-S.; Shevlin, S. A.; Woodley, S. M.; Kowalski, K.; Zwijnenburg, M. A. Modeling Excited States in TiO_2 Nanoparticles: On the Accuracy of a TD-DFT Based Description. *J. Chem. Theo. Comput.* **2014**, *10*, 1189-1199.

(36) Zade, S. S.; Zamoshchik, N.; Bendikov, M. From Short Conjugated Oligomers to Conjugated Polymers. Lessons from Studies on Long Conjugated Oligomers. *Acc. Chem. Res.* **2010**, *44*, 14-24.

(37) Baer, R.; Livshits, E.; Salzner, U. Tuned Range-Separated Hybrids in Density Functional Theory. *Ann. Rev. Phys. Chem.* **2010**, *61*, 85-109.

(38) Becke, A. D. Density-Functional Exchange-Energy Approximation with Correct Asymptotic Behavior. *Phys. Rev. A* **1988**, *38*, 3098.

(39) Casanovas, J.; Alemán, C. Comparative Theoretical Study of Heterocyclic Conducting Oligomers: Neutral and Oxidized Forms. *J. Phys. Chem. C* **2007**, *111*, 4823-4830.

(40) Lukeš, V.; Rapta, P.; Idzik, K. R.; Beckert, R.; Dunsch, L. Charged States of 1, 3, 5-Triazine Molecules as Models for Star-Shaped Molecular Architecture: A DFT and Spectroelectrochemcial Study. *J. Phys. Chem. B* **2011**, *115*, 3344-3353.

(41) Mishra, A. K.; Tandon, P. A Comparative Ab Initio and DFT Study of Polyaniline Leucoemeraldine Base and its Oligomers. *J. Phys. Chem. B* **2009**, *113*, 14629-14639.

(42) Petrova, J. N.; Romanova, J. R.; Madjarova, G. K.; Ivanova, A. N.; Tadjer, A. V. Fully Doped Oligomers of Emeraldine Salt: Polaronic Versus Bipolaronic Configuration. *J. Phys. Chem. B* **2011**, *115*, 3765-3776.

(43) Salzner, U. Quantitatively Correct UV-Vis Spectrum of Ferrocene with TDB3LYP. *J. Chem. Theo. Comput.* **2013**, *9*, 4064-4073.

(44) Ullah, H.; Ayub, K.; Ullah, Z.; Hanif, M.; Nawaz, R.; Shah, A. A.; Bilal, S. Theoretical Insight of Polypyrrole Ammonia Gas Sensor. *Synth. Met.* **2013**, *172*, 14-20.

(45) Ullah, H.; Shah, A. A.; Bilal, S.; Ayub, K. DFT Study of Polyaniline NH_3, CO_2 and CO Gas Sensors: Comparison with Recent Experimental Data. *J. Phys. Chem. C* **2013**, *117*, 23701-23711.

(46) Ullah, H.; Shah, A. A.; Ayub, K.; Bilal, S. Density Functional Theory Study of Poly (*O*-Phenylenediamine) Oligomers. *J. Phys. Chem. C* **2013**, *117*, 4069-4078.

(47) Zamoshchik, N.; Salzner, U.; Bendikov, M. Nature of Charge Carriers in Long Doped Oligothiophenes: The Effect of Counterions. *J. Phys. Chem. C* **2008**, *112*, 8408-8418.

(48) Bibi, S.; Ullah, H.; Ahmad, S. M.; Shah, A. A.; Bilal, S.; Tahir, A. A.; Ayub, K. Molecular and Electronic Structure Elucidation of Polypyrrole Gas Sensors. *J. Phys. Chem. C* **2015**, *119*, 15994-16003.

(49) Patra, A.; Agrawal, V.; Bhargav, R.; Bhardwaj, D.; Chand, S.; Sheynin, Y.; Bendikov, M. Metal Free Conducting Pedos, Pedot, and Their Analogues Via an Unusual Bromine-Catalyzed Polymerization. *Macromolecules* **2015**, *48*, 8760-8764.

(50) Patra, A.; Bendikov, M.; Chand, S. Poly (3, 4-Ethylenedioxyselenophene) and its Derivatives: Novel Organic Electronic Materials. *Acc. Chem. Res.* **2014**, *47*, 1465-1474.

(51) Li, M.; Sheynin, Y.; Patra, A.; Bendikov, M. Tuning the Electrochromic Properties of Poly (Alkyl-3, 4-Ethylenedioxyselenophenes) Having High Contrast Ratio and Coloration Efficiency. *Chem. Mater.* **2009**, *21*, 2482-2488.

(52) Patra, A.; Wijsboom, Y. H.; Zade, S. S.; Li, M.; Sheynin, Y.; Leitus, G.; Bendikov, M. Poly (3, 4-Ethylenedioxyselenophene). *J. Am. Chem. Soc.* **2008**, *130*, 6734-6736.

(53) Alberga, D.; Mangiatordi, G. F.; Labat, F.; Ciofini, I.; Nicolotti, O.; Lattanzi, G.; Adamo, C. Theoretical Investigation of Hole Transporter Materials for Energy Devices. *J. Phys. Chem. C* **2015**, *119*, 23890-23898.

(54) Risko, C.; Kushto, G.; Kafafi, Z.; Brédas, J.-L. Electronic Properties of Silole-Based Organic Semiconductors. *J. Chem. Phys.* **2004**, *121*, 18.

(55) Duan, Y. A.; Geng, Y.; Li, H. B.; Jin, J. L.; Wu, Y.; Su, Z. M. Theoretical Characterization and Design of Small Molecule Donor Material Containing Naphthodithiophene Central Unit for Efficient Organic Solar Cells. *J. Comput. Chem.* **2013**, *34*, 1611-1619.

(56) Coropceanu, V.; Cornil, J.; da Silva Filho, D. A.; Olivier, Y.; Silbey, R.; Brédas, J.-L. Charge Transport in Organic Semiconductors. *Chem. Rev.* **2007**, *107*, 926-952.

(57) Okawa, Y.; Akai-Kasaya, M.; Kuwahara, Y.; Mandal, S. K.; Aono, M. Controlled Chain Polymerisation and Chemical Soldering for Single-Molecule Electronics. *Nanoscale* **2012**, *4*, 3013-3028.

(58) Okur, S.; Salzner, U. Theoretical Modeling of the Doping Process in Polypyrrole by Calculating UV/Vis Absorption Spectra of Neutral and Charged Oligomers. *J. Phys. Chem. A* **2008**, *112*, 11842-11853.

(59) Ullah, H.; Shah, A.-u.-H. A.; Bilal, S.; Ayub, K. Doping and Dedoping Processes of Polypyrrole: DFT Study with Hybrid Functionals. *J. Phys. Chem. C* **2014**, *118*, 17819-17830.

(60) Park, S. H.; Roy, A.; Beaupre, S.; Cho, S.; Coates, N.; Moon, J. S.; Moses, D.; Leclerc, M.; Lee, K.; Heeger, A. J. Bulk Heterojunction Solar Cells with Internal Quantum Efficiency Approaching 100%. *Nat. Photon.* **2009**, *3*, 297-302.

(61) Wang, M.; Hu, X.; Liu, P.; Li, W.; Gong, X.; Huang, F.; Cao, Y. Donor–Acceptor Conjugated Polymer Based on Naphtho [1, 2-C: 5, 6-c] Bis [1, 2, 5] Thiadiazole for High-Performance Polymer Solar Cells. *J. Am. Chem. Soc.* **2011**, *133*, 9638-9641.

(62) Ayachi, S.; Mabrouk, A.; Alimi, K.; Bouachrine, M. *Photophysical Properties of Two New Donor-Acceptor Conjugated Copolymers and Their Model Compounds: Applications in Polymer Light Emitting Diodes (Pleds) and Polymer Photovoltaic Cells (Ppcs)*; INTECH Open Access Publisher, 2012.

(63) Li, L.; Huang, Y.; Peng, J.; Cao, Y.; Peng, X. Enhanced Performance of Solution-Processed Solar Cells Based on Porphyrin Small Molecules with a Diketopyrrolopyrrole Acceptor Unit and a Pyridine Additive. *J. Mater. Chem. A* **2013**, *1*, 2144-2150.

(64) Dou, L.; You, J.; Yang, J.; Chen, C.-C.; He, Y.; Murase, S.; Moriarty, T.; Emery, K.; Li, G.; Yang, Y. Tandem Polymer Solar Cells Featuring a Spectrally Matched Low-Bandgap Polymer. *Nat. Photon.* **2012**, *6*, 180-185.

(65) He, Y.; Chen, H.-Y.; Hou, J.; Li, Y. Indene− C60 Bisadduct: A New Acceptor for High-Performance Polymer Solar Cells. *J. Am. Chem. Soc.* **2010**, *132*, 1377-1382.

(66) Hou, J.; Guo, X. In *Organic Solar Cells*; Springer: 2013, p 17-42.

(67) Wang, F.; Zhang, B.; Li, Q.; Shi, Z.; Yu, L.; Liu, H.; Wang, Y.; Dai, S.; Tan, Z. a.; Li, Y. Management of the Light Distribution within the Photoactive Layer for High Performance Conventional and Inverted Polymer Solar Cells. *J. Mater. Chem. A* **2016**.

(68) Yang, Y. M.; Chen, W.; Dou, L.; Chang, W.-H.; Duan, H.-S.; Bob, B.; Li, G.; Yang, Y. High-Performance Multiple-Donor Bulk Heterojunction Solar Cells. *Nat. Photon.* **2015**, *9*, 190-198.

(69) Cheun, H.; Kim, J.; Zhou, Y.; Fang, Y.; Dindar, A.; Shim, J.; Fuentes-Hernandez, C.; Sandhage, K. H.; Kippelen, B. Inverted Polymer Solar Cells with Amorphous Indium Zinc Oxide as the Electron-Collecting Electrode. *Opt. Express* **2010**, *18*, A506-A512.

TOC Graphic